X-ray photoelectron spectroscopy study of the reduction and oxidation of uranium and cerium single oxide compared to (U-Ce) mixed oxide films

Eloirdi, R.; Cakir, P.; Huber, F.; Seibert, A.; Konings, R.; Gouder, T.

DOI
10.1016/j.apsusc.2018.06.148

Publication date
2018

Document Version
Final published version

Published in
Applied Surface Science

Applied Surface Science 457 (2018) 566–571

Contents lists available at ScienceDirect

Applied Surface Science

journal homepage: www.elsevier.com/locate/apsusc

Full Length Article

X-ray photoelectron spectroscopy study of the reduction and oxidation of uranium and cerium single oxide compared to (U-Ce) mixed oxide films

R. Eloirdi[a,*], P. Cakir[a,b], F. Huber[a], A. Seibert[a], R. Konings[a,b], T. Gouder[a]

[a] European Commission, Joint Research Centre, Directorate of Nuclear Safety and Security, P.O. Box 2340, D-76125 Karlsruhe, Germany
[b] Department of Radiation Science and Technology, Delft University of Technology, Mekelweg 15, 2629 JB Delft, The Netherlands

ARTICLE INFO

Keywords:
Uranium
Cerium
Thin film
Mixed oxide
Redox
XPS

ABSTRACT

Thin films of uranium cerium mixed oxides $U_xCe_{1-x}O_{2\pm y}$ have been prepared by DC sputtering and characterized by X-ray photoelectron spectroscopy (XPS). Reduction and oxidation properties were analysed by exposing the films to atomic hydrogen and to atomic oxygen, respectively. Possible interaction between uranium and cerium were investigated by comparing the compounds to the single oxides of cerium and uranium. Uranium seems to promote the reduction of cerium. Conversely cerium promotes oxidation of uranium. Under our deposition conditions, it was not possible to produce pure U(IV) together with pure Ce(IV). The synthesis of U_2O_5 with U(V) cannot be obtained directly by DC sputtering, whereas with addition of cerium, U(V) seems to be stabilized and obtained more easily. This can be related to a charge transfer between Ce(IV) and U(IV).

1. Introduction

The safety assessment of nuclear waste disposal in deep geological repositories requires an understanding of the corrosion behaviour of spent nuclear fuel (SNF). In particular the knowledge about the dissolution of the UO_{2+x} matrix in the groundwater is crucial, as it can be linked to concomitant release of radionuclides produced during fission [1,2]. The chemical properties of the spent fuel are strongly related to the oxidation state of uranium and thus to any parameter having influence on it [3]. It is well known that the solubility of uranium oxide increases sharply with the oxidation state, but it is also affected by the presence of other elements, transuranium elements or fission products. The effect of plutonium is of particular interest, as mixed uranium-plutonium oxide (MOX) is used as fuel in numerous nuclear reactors, and accumulates as spent nuclear fuel.

In a previous work we focused on the effect of thorium, on $(U_x,Th_{1-x})O_2$ dissolution [4]. Thorium has only one stable oxidation state (IV), therefore, only uranium can change oxidation state, and the system is relatively simple. In the present paper we study the influence of cerium, which has two stable oxidation states, (III) and (IV). Since these oxidation states of cerium are similar to plutonium [5–7] the mixed oxide with uranium can be investigated as surrogate for (U-Pu) mixed oxides. Cerium also forms as a fission product during reactor operation, together with other lanthanide elements, and thus be considered as spent fuel model as well. Cerium oxide is also a candidate for hydrogen production by concentrated solar power using thermochemical cycles for water splitting [8,9] because of its redox behaviour and high temperature stability. In this frame also (U-Ce) mixed oxides were investigated [10].

In this work, we investigate the interaction of uranium and cerium in mixed oxides using thin film model surfaces produced in-situ by DC sputtering. Sputter deposition is a versatile method for producing samples with different U/Ce stoichiometries and oxygen content (O/M ratios). In contrast to real spent fuel, which is very complex, doped films allow focussing on one single element (Ce) and performing a single effect study. Since the interaction of the environment with spent fuel takes place at the surface, this process can be perfectly reproduced by using thin films.

DFT studies have shown that when CeO_2 is mixed with UO_2, a charge transfer takes place between the U(IV) and Ce(IV) leading to U (V) and Ce(III) [11]. This is corroborated by several experimental studies on (U-Ce) mixed oxide using XPS, in which the surface oxidation states have been analysed. Bera et al. [12] found Ce(III) alongside of U (IV), U(V) and U(VI). XPS measurements and analysis of the oxidized and reduced $Ce_xU_{1-x}O_{2\pm y}$ were performed by Al-Salik et al. [13]. While uranium was reduced from U(VI) to U(V) to U(IV) during Ar^+ ions sputtering, cerium was more sensitive to reduction in the mixed oxide than pure CeO_2. This shows that uranium promotes cerium reduction.

Even though there have been several studies on the redox behaviour of pure cerium and uranium oxide thin films, research on the uranium cerium mixed oxide thin films has so far not been performed, in contrast

* Corresponding author.
E-mail address: rachel.eloirdi@ec.europa.eu (R. Eloirdi).

https://doi.org/10.1016/j.apsusc.2018.06.148
Received 4 April 2018; Received in revised form 4 June 2018; Accepted 16 June 2018
Available online 18 June 2018

to bulk systems [5,10,12,13].

In this work, we study the redox reactions on (U-Ce) mixed oxide surfaces upon exposure to atomic hydrogen and oxygen, respectively. The use of highly reactive atomic species ($O^{\cdot}$ and $H^{\cdot}$) for oxidation and reduction of the film surfaces allows reproducing redox processes in the repository, triggered by alpha radiolysis of groundwater, creating strong oxidants (H_2O_2, $H_2O^{\cdot}$, O_2) and reductants (H_2, $H^{\cdot}$, e^-) [14]. Reaction with the more common molecular species (O_2 and H_2) under vacuum conditions (where electron spectroscopy is done) fails producing these effects because of the very low reactivity of these species.

In the following, we first discuss reference spectra of CeO_2, Ce_2O_3, UO_2, U_2O_5 and UO_3 thin films and the deposition of (U-Ce) mixed oxide. Second, reduction by atomic hydrogen at room temperature of CeO_2 and UO_3 will be compared to (U-Ce) mixed oxide film (ratio U/Ce ~ 1), to understand the effect on the redox behaviour in the solid solution as claimed in literature [13]. In the third part, oxidation of Ce_2O_3, and U_2O_5 have been performed by exposure to atomic oxygen at 573–673 K, and compared to a (U-Ce) mixed oxide film (ratio U/Ce ~ 0.05). The high temperature was chosen to enable diffusion of oxygen into deeper layers and to achieve a homogeneously oxidized film. We will discuss the redox states of uranium and cerium in the mixed oxide and more specifically the effect of Ce(III) on the uranium valence , and compare to other Ln(III) cations [15–18].

2. Experimental

The thin films of $U_xCe_{1-x}O_{2\pm y}$ (x = 0 to 1) were prepared in-situ by direct current reactive co-sputtering from cerium and uranium metal targets in a gas mixture of Ar (6N) and O_2 (6N). The oxygen concentration in the films was adjusted by changing the O_2 partial pressure (10^{-4} Pa–5×10^{-3} Pa), while the Ar partial pressure was maintained at 5×10^{-3} mbar. The composition of the films was controlled by changing the respective target voltages for the uranium and cerium targets.

The thin films were deposited for 120 s with a deposition rate of about 1 Å/s, at room temperature on silicon wafer (1 0 0) substrates, which were cleaned by Ar ion sputtering (4 keV) for 10 min, and subsequently annealed under UHV at 773 K for 5 min. The plasma in the diode source was maintained by injection of electrons of 25–50 eV energy (triode setup), to work at low Ar pressure in absence of stabilizing magnetic fields.

Atomic oxygen ($O^{\cdot}$) and hydrogen ($H^{\cdot}$) were generated in an electron cyclotron resonance (ECR) Plasma Source Gen I from Tectra GmbH, Frankfurt/M. The atom flux is specified to $> 10^{16}$ atoms/cm^2/s, corresponding to an exposure of roughly 10 Langmuir/s (i.e. 1.33×10^{-3} Pa/s).

High resolution X-ray photoelectron spectroscopy (XPS) measurements were performed using a Phoibos 150 hemispherical analyser. Al K_α (E = 1486.6 eV) radiation was produced by a XRC-1000 micro-focus source, equipped with a monochromator and operating at 120 W. The background pressure in the analysis chamber was around 2×10^{-10} mbar. The spectrometer was calibrated using the Au-$4f_{7/2}$ line (83.9 eV) and Cu-$2p_{3/2}$ (932.7 eV) of metallic gold and copper standards. Photoemission spectra were taken at room temperature. Data analyses were performed using CasaXPS software.

All the films produced and used for this study are never in contact with the laboratory atmosphere. The transfer of the different films from preparation chamber to analyses chamber is made under UHV and by remote control using the Labstation developed at JRC Karlsruhe.

3. Results

3.1. Reference spectra of the cerium and uranium single oxides, and (U-Ce) mixed oxide deposition

The two cerium oxides CeO_2 and Ce_2O_3 were obtained by sputter deposition at the appropriate O_2 partial pressure.

Table 1
Binding energy of Ce-*3d* peaks present in Ce_2O_3 and CeO_2 thin films.

Ce(III)	Initial → Final state	Binding energy [eV]	Ce(IV)	Initial → Final state	Binding energy [eV]
V^0	$3d^{10}4f^1 \rightarrow$	881.6	V	$3d^{10}4f^0(5d6s)^0 \rightarrow$	882.3
W^0	$3d^94f^2(5d6s)^0$	900	W	$3d^94f^1(5d6s)^0$	900.7
V′	$3d^{10}4f^1 \rightarrow$	886	V″	$3d^{10}4f^0\ (5d6s)^0 \rightarrow$	889
W′	$3d^94f^1(5d6s)^1$	904.6	W″	$3d^94f^0(5d6s)^1$	907.3
			V‴	$3d^{10}4f^0\ (5d6s)^0 \rightarrow$	898.1
			W‴	$3d^94f^0(5d6s)^0$	916.5

The Ce-*3d* spectra are rather complex [19–21] due to the coexistence of different final states, well screened, poorly screened and unscreened peaks are observed at different binding energies (BE). The ground state configurations of cerium are $[Xe]4f^1(5d6s)^3$ for Ce^0, $[Xe]4f^1(5d6s)^0$ for Ce^{3+} and $[Xe]4f^0(5d6s)^0$ for Ce^{4+}. The photoemission process then leads to the typical final state screening picture, where the core hole is screened by population of the *4f* states (good screening), 5d6s (poor screening) and no population at all (non-screening). The corresponding photoemission peaks for Ce(III) and Ce(IV) are summarized in Table 1. These values are in very good agreement with spectra obtained in literature [19,21–24].

Fig. 1 shows the Ce-*3d* spectra together with the O-*1s* spectra corresponding to Ce_2O_3 (blue curves) and CeO_2 (red curves) films. Ce_2O_3 displays four peaks for Ce-*3d*, labelled W^0, W′ and V^0, V′ assigned to $3d_{3/2}$ and $3d_{5/2}$ respectively. In CeO_2 the six peaks, W, W″, W‴ and V, V″, V‴ are assigned to $3d_{3/2}$ and $3d_{5/2}$ respectively. The peak at 916.5 eV BE (W‴) is a clear indicator for Ce(IV) because it does not superimpose with any Ce(III) line – it is not present in the spectrum of Ce_2O_3. It corresponds to the unscreened Ce-$3d_{3/2}$ final state of Ce(IV). However, there is no clear linear dependence between Ce^{4+} concentration and W‴ intensity [25].

The corresponding O-*1s* main line of CeO_2 and Ce_2O_3 lie at 529.7 eV and 530.4 eV BE, respectively. The O-*1s* line of Ce_2O_3 has a shoulder on its high binding energy side while for CeO_2, the peak is relatively symmetric. Although this shoulder could a priori be explained by the oxygen from the oxidized silicon substrate interface [19] which is in contact with the Ce_2O_3 thin film, this has been rejected because the BE difference with the main peak is too low relatively to the expected value for O-Si substrate lines in the present study. The shoulder has also been attributed to H_2O adsorbed on defect sites [23,26]. In general, water chemisorbed on oxides gives such high BE shoulder [27]. However, it has been shown that even at a temperature of 645 K the shoulder does not totally disappear [23]. Pfau et al. [21] have linked this shoulder to

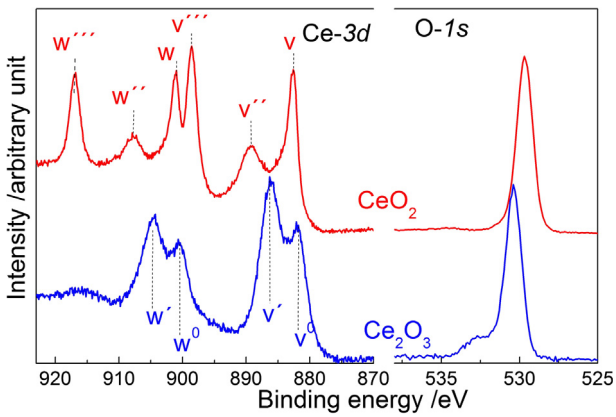

Fig. 1. Ce-*3d* and O-*1s* core level spectra present in CeO_2 (red) and in Ce_2O_3 (blue) films. (For interpretation of the references to colour in this figure legend, the reader is referred to the web version of this article.)

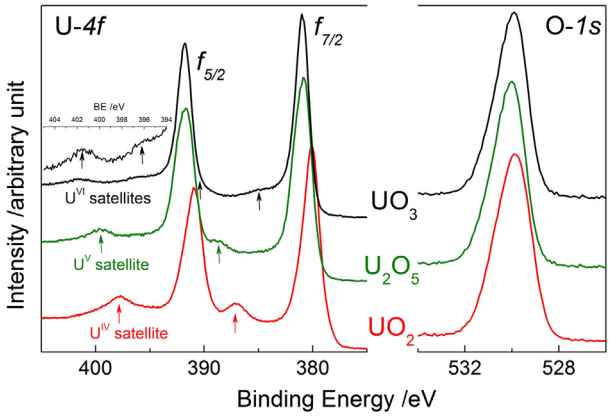

Fig. 2. U-*4f* and O-*1s* core level spectra present in UO_2 (red), U_2O_5 (green) and in UO_3 (black) films _insert. Satellite peaks of UO_3. (For interpretation of the references to colour in this figure legend, the reader is referred to the web version of this article.)

vacancies or disorder induced by the presence of Ce(III) in the sample. Ce_2O_3 deposition at ambient temperature leads to more defects, because of the absence of thermal annealing, as the atoms do not have the energy to diffuse and organize at the surface of the substrate. In this study we always observe this shoulder when Ce_2O_3 is present in the mixed oxide.

Fig. 2 compares the U-*4f* and O-*1s* core level spectra of UO_2, U_2O_5 and UO_3 films. Unlike UO_2, Ce_2O_3 and CeO_2 which can be produced directly by DC sputtering by varying the O_2 partial pressure, thin films of U_2O_5 and UO_3 require further oxidation and reduction treatment with atomic oxygen and atomic hydrogen to be produced. To get UO_3, post-deposition exposure to atomic oxygen at high temperature, 673 K, is necessary. U_2O_5 is obtained by reducing with atomic hydrogen the UO_3 films, kept at the same temperature of 673 K [28].

Spectra show the spin-orbit split final states of U-$4f_{5/2}$ and U-$4f_{7/2}$ with $\Delta E = 10.8$ eV. The main lines undergo a strong chemical shift between UO_2 and U_2O_5 ($\Delta E = 0.8$ eV) and a weaker one between U_2O_5 and UO_3 ($\Delta E = 0.2$ eV). The main lines are accompanied by characteristic satellites at higher binding energy. Table 2 summarizes the binding energy of the main peaks and the linked satellite peaks for U (IV), U(V) and U(VI). The satellite peaks play an important role in the assignment of the oxidation state of uranium. The energy difference (ΔE) between satellite and main line steadily increase with the oxidation state. The satellite has been attributed to the energy loss of the photoelectrons due to excitation of an O-*2p* → U-$5f_{unoccupied}$ electron transition. However, the correlation between the satellite energies and intensities and inter-atomic effects 0r environmental coordination is still not clear.

Fig. 3 shows the U-*4f*, Ce-*3d* and O-*1s* spectra of uranium rich $U_{0.8}Ce_{0.2}O_{2-x}$ films co-deposited at low (traces of oxygen) and at high oxygen partial pressure. The fitting of Ce-*3d* and U-*4f* peaks was done by using CasaXPS. Shirley algorithm for inelastic background subtraction [29] and Gaussian-Lorentzian profile were applied for the fitting of the peaks. U/Ce and M/O were calculated using the ratios between the respective peaks. Deposition at zero oxygen pressure still produces oxide films (Fig. 3, black curves), because of the residual oxidation of the targets from previous depositions and we did not especially seek producing metal films. The film contains U(IV), as shown by the *4f*-satellite at $\Delta E = 6.8$ eV (Table 2), and Ce(III), as shown by the characteristic *3d* spectrum (compare to Fig. 1). The corresponding O-*1s* spectrum has the main line together with the high BE shoulder, which was previously observed for Ce_2O_3. At higher oxygen partial pressure, uranium oxidizes further as shown by the appearance of a U-*4f* satellite at $\Delta E = 7.8$ eV, characteristic for U(V) (Table 2). Cerium is partially oxidized into Ce(IV). The O-*1s* peak shifts to lower binding energy and the high BE shoulder tends to disappear, resembling again the spectrum of CeO_2. The shift, which also occurs for Ce-*3d* and U-*4f* (rigid shift), is attributed to the decrease of the Fermi-energy as result of further surface oxidation.

It was not possible to obtain solely Ce(IV) together with U(IV). Even partial oxidation of Ce(III) only takes place when U^{4+} also oxidizes. This seems to reflect the chemical equilibrium situation at the surface, because during sputter deposition the impinging clusters bring enough energy with them to be organized in a stable configuration.

Table 2
Binding energy of O-*1s*, U-$4f_{7/2}$, U-$4f_{5/2}$ and ΔE of U-$4f_{5/2}$ satellite peak present in UO_2, U_2O_5 and UO_3.

	O-*1s* [eV]	U-$4f_{7/2}$ [eV]	U-$4f_{5/2}$ [eV]	ΔE [eV] U-$4f_{5/2}$-satellites	
UO_2	529.9 ± 0.1	380.1 ± 0.1	390.9 ± 0.1	6.8 ± 0.2	
U_2O_5	530.0 ± 0.1	380.8 ± 0.1	391.7 ± 0.1	7.8 ± 0.1	
UO_3	529.9 ± 0.1	381.0 ± 0.1	391.8 ± 0.1	9.7 ± 0.1	4.1 ± 0.1

3.2. Reduction process with atomic hydrogen

Reduction of CeO_2 and uranium higher oxides, as bulk materials and thin films, are described in detail in the literature [13,19,30]. Reduction may occur by thermal decomposition (oxygen desorption), Ar^+ sputtering (preferential removal of oxygen) or reaction with hydrogen (water formation and desorption).

In Fig. 4, spectra of Ce-*3d*, U-*4f* and O-*1s* along the reduction of pure CeO_2 (Fig. 4A) and pure UO_3 (Fig. 4B) films are reported and compared to the reduction of $U_{0.45}Ce_{0.55}O_{2+x}$ by atomic hydrogen (Fig. 4C).

Fig. 4A displays the spectra of CeO_2 obtained after deposition (black curve), and after exposure to atomic hydrogen at room temperature (green curve) and subsequent heating at 473 K (blue curve). Exposure to atomic hydrogen at ambient temperature has only a slight effect on the Ce^{4+}/Ce^{3+} ratio measured by XPS (10 atomic layers): the intensity of the Ce^{4+} signal at 916 eV does not decrease and conversely the intensity of the Ce^{3+} line at about 904.6 eV (W') does not increase. Subsequent heat treatment at 473 K did not change much the Ce^{4+}/Ce^{3+} ratio either. Another interesting sign of reduction on surface is the shoulder at higher BE appearance on the O-*1s* spectrum (inset Fig. 4A). This has been discussed many times in literature [23,31]. It is concluded that the surface hydroxyl appears as sign of oxygen vacancy and result of the reduction via break of M—O bond. The existence of OH^- emission was also found in reductions of PuO_2 to Pu_2O_3 [32]. In our study, we can say that the peak intensity of the shoulder in O-*1s* signal does not change much during the reduction process at room temperature followed by heating at 473 K. Surface reduction thus takes place more efficiently when the sample is simultaneously heated to 473 K and exposed to atomic hydrogen (Fig. 4A, red curve). Decrease of the Ce^{4+} signal at 916.5 eV signal is in this condition stronger. We explain the stronger reaction by the enhanced mobility of hydrogen and/or oxygen. Diffusion of H in the bulk has been confirmed by XPS measurements made on grazing incidence (not reported here) showing a constant intensity peak of Ce(III) for room and for higher temperature. The limiting step for the lower near surface layers reduction is linked to the diffusion of hydrogen and/or oxygen through the lattice.

Fig. 4B shows U-*4f* core level spectra of UO_3 before and after exposure to atomic hydrogen at ambient temperature. The changing U-*4f* satellite energies (see Table 2) show that U(VI) is reduced into U(V), i.e. UO_3 into U_2O_5. Reduction to U_2O_5 is complete with the information depth of XPS, with a mean information depth of 10 monolayers.

Fig. 4C shows the reaction of a mixed (U-Ce) oxide when exposed to atomic hydrogen at room temperature. In the mixed oxide both elements can change their oxidation state and the question is whether uranium can promote the reduction of cerium. The initial deposition (black curve) shows the characteristic U-*4f* peaks of U(VI) with some

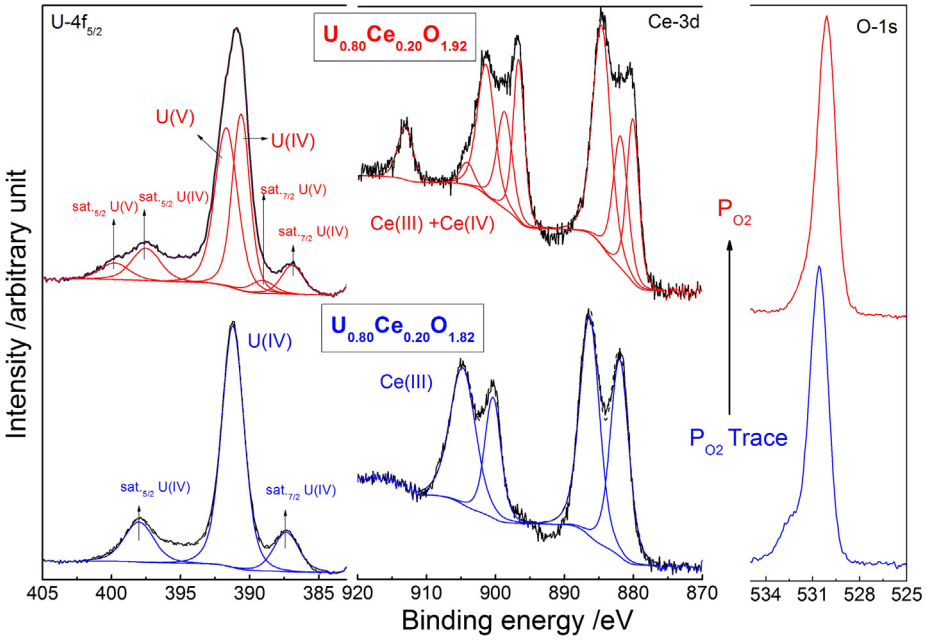

Fig. 3. U-*4f*, Ce-*3d* and O-*1s* of $U_{0.80}Ce_{0.20}$Oxide, effect of PO_2 increase during co-deposition.

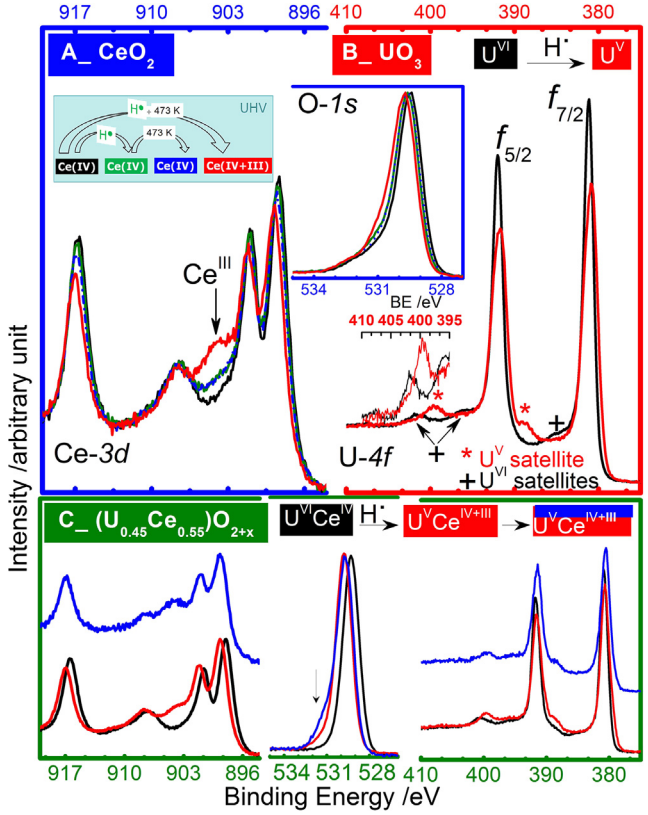

Fig. 4. Ce-*3d* and U-*4f* before and after reduction with atomic hydrogen obtained on A_ CeO_2, B_ UO_3 and C_ $U_{0.45}Ce_{0.55}O_{2+x}$. Insert_O-*1s* of CeO_2.

trace of U(V) and a Ce-*3d* peak typical for Ce(IV). The O-*1s* peak is of symmetrical shape. Deposition was performed at highest possible oxygen partial pressure. The high limit is imposed by the oxidation of the targets during sputter deposition, which eventually disrupts the plasma. It should be noticed that for uranium deposition alone (see above), the highest uranium oxidation that could be reached in the films was UO_{2+x} with a mixture of U(IV) + U(V). In presence of cerium, U(VI) is obtained as main valence state. Co-deposition with cerium as Ce(IV) thus seems to enhance uranium oxidation further to U(VI) after deposition by DC sputtering. The presence of both trivalent and tetravalent states of cerium is expected by the charge transfer reaction between U and Ce as proposed by Griffiths et al. [33] as follows.

$$Ce^{4+} + U^{4+} \rightarrow Ce^{3+} + U^{5+}$$

A charge-transfer process or orbital hybridization [34–36] has also been reported for the known "cerium-uranium blue" colour of some CeO_2-UO_2 solid solutions. Magnetic studies [36] of CeO_2-UO_2 solid solutions were interpreted in terms of partial charge transfer.

When the surface is exposed to atomic hydrogen at room temperature (RT), uranium is fully reduced into U(V) (red curve), as for pure UO_3. Also, Ce(IV) is reduced into Ce(III) even though to a lesser extent. This stands in contrast to pure CeO_2, which was hardly reduced. Obviously, cerium reduction is enhanced by uranium. Upon reduction the Ce-*3d* peaks shift to higher BE by 0.5 eV. A similar shift is observed for the O-*1s* peak. It is attributed to the increase of the Fermi-energy upon formation of Ce_2O_3 and reduction of UO_3, and as consequence of negative charging of the surface. As after effect all photoemission peaks rigidly shift to higher binding energy (Ce-*3d*, O-*1s*). For the U-*4f* peak, this shift is compensated by the reduction of U(VI) to U(V) which leads to a chemical shift of the U-*4f* line to about 0.2–0.5 eV lower binding energy. When spectra are taken at grazing incidence (blue curves), the Ce(III) signal at about 904.6 eV increases slightly showing reduction to take place mainly at the top surface. Also, the high BE shoulder of the O-*1s* peak is increasing (arrow O-*1s* Fig. 4C), pointing to the presence of of Ce_2O_3.

For better comparison, the Ce-*3d* spectra of CeO_2 and $U_{0.45}Ce_{0.55}O_{2+x}$ after reaction with hydrogen are superposed with normalised intensities in Fig. 5. The mixed oxide has a more reduced Ce (III) signal. The presence of uranium seems to facilitate the reduction of cerium at room temperature. The grazing incidence measurement shows that the cerium reduction is more pronounced at the surface. The corresponding reduction of uranium from U(VI) into U(V) is well extending into the layers underneath.

Similar results are obtained by other authors for bulk samples of mixed uranium-cerium oxides who observed that cerium is more prone to reduction when mixed with uranium [10,13].

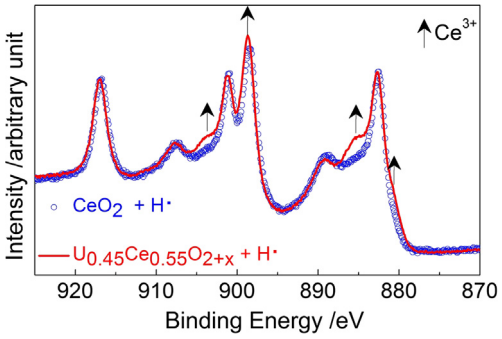

Fig. 5. Ce-*3d* core level spectra of CeO_2 and $U_{0.45}Ce_{0.55}O_{2+x}$ after the exposure to atomic hydrogen at room temperature.

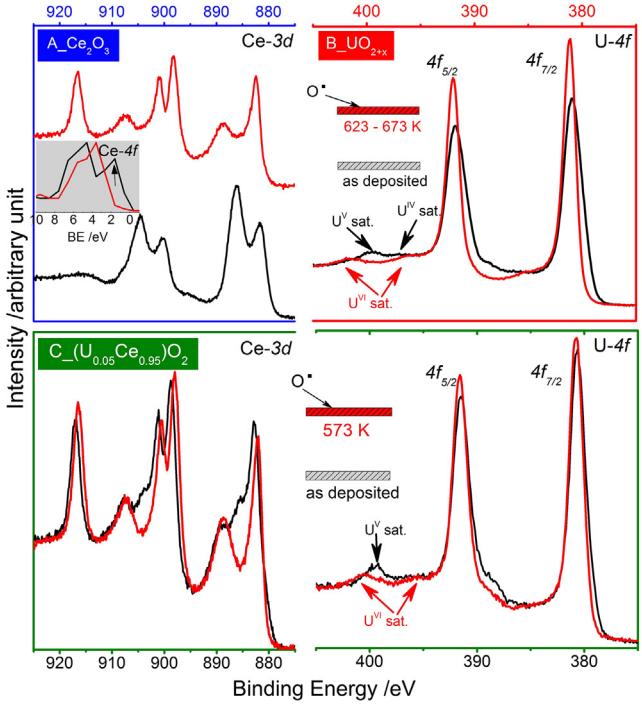

Fig. 6. Ce-*3d* and U-*4f* before and after oxidation with atomic oxygen at about 600 K obtained on A_Ce_2O_3, B_U_2O_5 and C_of $U_{0.05}Ce_{0.95}O_2$ after deposition and after oxidation with atomic oxygen at 573 K.

3.3. Oxidation process with atomic oxygen

Fig. 6 displays the Ce-*3d* and U-*4f* core level spectra along the oxidation with atomic oxygen of Ce_2O_3 (Fig. 6A) and UO_{2+x} (Fig. 6B) compared to the oxidation of $U_{0.05}Ce_{0.95}O_2$ (Fig. 6C). $U_{0.05}Ce_{0.95}O_2$ film is deposited at the highest possible oxygen pressure (limited by U and Ce target oxidation).

The oxidation of Ce_2O_3 by atomic oxygen at 623–673 K leads to pure CeO_2 as indicated by the characteristic Ce-*3d* spectrum and by the absence of Ce-*4f* at about 1 eV (Fig. 6A_insert). Oxidation of UO_{2+x} by atomic oxygen leads to the formation of UO_3. The absence of U^{IV} or U^{V} is demonstrated by the absence of the localized U*5f* emission [28].

After deposition of $U_{0.05}Ce_{0.95}O_2$ (black curves), cerium is present as a mixture with mostly Ce^{4+}, while uranium is exclusively U(V), as shown by the satellite at $\Delta E = 7.8$ eV. While we cannot obtain directly U_2O_5 by DC sputtering, it is interesting to see that in addition to cerium, a single oxidation state of uranium as U(V) can be directly obtained by DC sputtering. This can be due to charge transfer between uranium and cerium, stabilizing U(V) at the extent of pure and single U(IV) together with Ce(IV).

After oxidation of $U_{0.05}Ce_{0.95}O_2$ with atomic oxygen, cerium is completely oxidised into Ce^{4+} as shown by the absence of Ce-*4f* peak at about 1 eV [37] while uranium is oxidised in U^{+6} with still some trace of U^{+5} as observed by a weak shoulder at low BE of U-$4f_{5/2}$ linked to U^{+5} satellite peak. Compared to binary uranium oxide UO_{2+x} (Fig. 6B) which oxidized completely to U(VI) in the mixed oxide , the oxidation of uranium into U(VI) is not complete, which may be linked to the presence of Ce(III) present initially as it has been reported in literature relatively to Ln(III) [15–17] which decrease the trend of uranium to oxidise into U(VI).

4. Conclusion

We studied the surface reactivity of (U-Ce) mixed oxides towards atomic hydrogen and atomic oxygen. The redox behaviour of the mixed oxides was compared to that of the binary cerium and uranium oxides. Goal was to detect a possible mutual influence between uranium and cerium on their reactivity. Two questions were addressed, first if uranium has an influence on the reduction of Ce(IV) into Ce(III), second, whether Ce(III) could inhibit uranium oxidation to U(VI) formation, as was reported in literature for other Ln(III) cations [15–18].

Reference spectra of the single oxides were taken using CeO_2, Ce_2O_3, UO_2, U_2O_5 and UO_3 thin films. Both cerium oxides could be deposited directly by sputter deposition using the appropriate oxygen pressure. In the U-O system only UO_2 can be prepared directly by DC sputtering. At maximum oxygen partial pressure, deposition of UO_{2+x} is obtained, containing a mixture of U^{4+} and U^{5+}. The higher uranium oxides U_2O_5 and UO_3 representing the single state U(V) and U(VI) valence states, need post-deposition treatment with atomic oxygen at 673 K.

In mixed oxide films uranium, with mainly U^{6+} or mainly U^{5+} could be deposited directly without post-deposition oxidation necessary for single uranium oxide. This shows a higher reactivity of uranium towards oxygen when co-deposited with cerium and which can be linked to charge transfer between uranium and cerium.

Surface reaction with atomic hydrogen at room temperature was studied. CeO_2, UO_3 were compared to (U, Ce) mixed oxide system (ratio U/Ce ~ 1). It was shown that uranium promotes the reduction of cerium, as claimed in literature: at room temperature cerium is partially reduced to Ce(III) while in the same condition pure CeO_2 hardly reduces. Measurements at grazing incidence of the MOX showed that the cerium reduction is more pronounced at the surface. The corresponding reduction of uranium from U(VI) into U(V) is well extending into the layers underneath. The reduction of the (U-Ce) mixed oxide is thus a complex and incongruent process.

Surface oxidation with atomic oxygen at 573–673 K of (U, Ce) mixed oxide system (ratio U/Ce ~ 0.05) was compared to binary oxides Ce_2O_3 and U_2O_5 films. It was demonstrated that while uranium in U_2O_5 is completely oxidised to UO_3 as expected, uranium in the mixed oxide present initially as U(V) was not completely oxidised to U(VI), keeping some traces of U(V). The result might be linked to the temperature which was kept below 600 K.

It was so far not possible to form mixtures of U(IV) and Ce(IV) by co-deposition: U(V) always formed together with Ce(III), while Ce(IV) only formed in presence of U(V) or U(VI).

Acknowledgements

P. Cakir acknowledges the European Commission for support in the frame of the Training and Mobility of Researchers programme.

References

[1] H. Kleykamp, The chemical state of the fission products in oxide fuels, J. Nucl. Mater. 131 (1985) 221–246, http://dx.doi.org/10.1016/0022-3115(85)90460-X.
[2] L.H. Johnson, D.W. Shoesmith, Spent Fuel, in: W.B. Lutze, R.C. Ewing (Eds.),

Radioact, Waste Forms Futur, Amsterdam, The Netherlands, 1988, p. 635.
[3] I. Grenthe, J. Fuger, R.J.M. Konings, R.J. Lemire, A.G. Muller, C. Nguyen-Trung Cregu et al., Chemical Thermodynamics of Uranium, North Holland, Amsterdam, 1992.
[4] P. Cakir, R. Eloirdi, F. Huber, R.J.M. Konings, T. Gouder, Thorium effect on the oxidation of uranium: Photoelectron spectroscopy (XPS / UPS) and cyclic voltammetry (CV) investigation on $(U_{1-x}Th_x)O_2$ (x = 0 to 1) thin films, Appl. Surf. Sci. 393 (2017) 204–211, http://dx.doi.org/10.1016/j.apsusc.2016.10.010.
[5] K. Suresh Kumar, T. Mathews, H. Nawada, N. Bhat, Oxidation behaviour of uranium in the internally gelated urania–ceria solid solutions – XRD and XPS studies, J. Nucl. Mater. 324 (2004) 177–182, http://dx.doi.org/10.1016/j.jnucmat.2003.09.014.
[6] P. Martin, M. Ripert, T. Petit, T. Reich, C. Hennig, F. D'Acapito, et al., A XAS study of the local environments of cations in (U, Ce)O_2, J. Nucl. Mater. 312 (2003) 103–110, http://dx.doi.org/10.1016/S0022-3115(02)01590-8.
[7] D.I.R. Norris, P. Kay, Oxygen Potential and Lattice Parameter Measurements in (U, Ce)O_{2-x}, J. Nucl. Mater. 116 (1983) 184–194.
[8] H. Kaneko, T. Miura, H. Ishihara, S. Taku, T. Yokoyama, H. Nakajima, et al., Reactive ceramics of CeO_2–MO_x (M = Mn, Fe, Ni, Cu) for H_2 generation by two-step water splitting using concentrated solar thermal energy, Energy 32 (2007) 656–663, http://dx.doi.org/10.1016/j.energy.2006.05.002.
[9] S. Abanades, G. Flamant, Thermochemical hydrogen production from a two-step solar-driven water-splitting cycle based on cerium oxides, Sol. Energy 80 (2006) 1611–1623, http://dx.doi.org/10.1016/j.solener.2005.12.005.
[10] I. Al-Shankiti, F. Al-Otaibi, Y. Al-Salik, H. Idriss, Solar thermal hydrogen production from water over modified CeO_2 materials, Top. Catal. 56 (2013) 1129–1138, http://dx.doi.org/10.1007/s11244-013-0079-1.
[11] B.E. Hanken, C.R. Stanek, N. Grønbech-Jensen, M. Asta, Computational study of the energetics of charge and cation mixing in $U_{1-x}Ce_xO_2$, Phys. Rev. B 84 (2011) 85131, http://dx.doi.org/10.1103/PhysRevB.84.085131.
[12] S. Bera, V.K. Mittal, R. Venkata Krishnan, T. Saravanan, S. Velmurugan, K. Nagarajan, et al., XPS analysis of $U_xCe_{1-x}O_{2+y}$ and determination of oxygen to metal ratio, J. Nucl. Mater. 393 (2009) 120–125, http://dx.doi.org/10.1016/j.jnucmat.2009.05.015.
[13] Y. Al-Salik, I. Al-Shankiti, H. Idriss, Core level spectroscopy of oxidized and reduced $Ce_xU_{1-x}O_2$ materials, J. Electron Spectros. Relat. Phenom. 194 (2014) 66–73, http://dx.doi.org/10.1016/j.elspec.2013.11.013.
[14] G.R. Choppin, J.-O. Liljenzin, J. Rydberg, Radiochemistry and Nuclear Chemistry, Butterworth-Heinemann, 2002.
[15] N. Liu, Electrochemical and Modelling Studies on Simulated Spent Nuclear Fuel Corrosion under Permanent Waste Disposal Conditions, Electron. (Thesis Diss. Repos.), 2017. https://ir.lib.uwo.ca/etd/4412.
[16] J.-G. Kim, Y.-K. Ha, S.-D. Park, K.-Y. Jee, W.-H. Kim, Effect of a trivalent dopant, Gd^{3+}, on the oxidation of uranium dioxide, J. Nucl. Mater. 297 (2001) 327–331, http://dx.doi.org/10.1016/S0022-3115(01)00639-0.
[17] M. Razdan, D.W. Shoesmith, Influence of trivalent-dopants on the structural and electrochemical properties of uranium dioxide (UO_2), J. Electrochem. Soc. 161 (2013) H105–H113, http://dx.doi.org/10.1149/2.047403jes.
[18] H. He, K. O 'Neil, O. Semenikhin, D.W. Shoesmith, The Influence of Rare-Earth Doping and Non-Stoichiometry on the Corrosion of Uranium Dioxide, 2012.
[19] P. Bera, C. Anandan, Growth, structural characterization and interfacial reaction of magnetron sputtered CeO_2 thin films on different substrates, Surf. Rev. Lett. 21 (2014) 1450054, http://dx.doi.org/10.1142/S0218625X14500541.
[20] D.D. Koelling, A.M. Boring, J.H. Wood, The electronic structure of CeO_2 and PrO_2, Solid State Commun. 47 (1983) 227–232.
[21] A. Pfau, K.D. Schierbaum, The electronic structure of stoichiometric and reduced CeO, surfaces: an XPS, UPS and HREELS study, Surf. Sci. 6028 (1994) 71–80.
[22] M.A. Henderson, C.L. Perkins, M.H. Engelhard, S. Thevuthasan, C.H.F. Peden, Redox properties of water on the oxidized and reduced surfaces of CeO_2 (1 1 1), Surf. Sci. 526 (2003) 1–18, http://dx.doi.org/10.1016/S0039-6028(02)02657-2.
[23] S.M.F. Shahed, T. Hasegawa, Y. Sainoo, Y. Watanabe, N. Isomura, A. Beniya, et al., STM and XPS study of CeO_2 (111) reduction by atomic hydrogen, Surf. Sci. 628 (2014) 30–35, http://dx.doi.org/10.1016/j.susc.2014.05.008.
[24] D.R. Mullins, The surface chemistry of cerium oxide, Surf. Sci. Rep. 70 (2015) 42–85, http://dx.doi.org/10.1016/j.surfrep.2014.12.001.
[25] M. Romeo, K. Bak, J. El Fallah, F. Le Normand, L. Hilaire, XPS Study of the reduction of cerium dioxide, Surf. Interface Anal. 20 (1993) 508–512, http://dx.doi.org/10.1002/sia.740200604.
[26] Y. Lykhach, V. Johánek, H.A. Aleksandrov, S.M. Kozlov, M. Happel, T. Skála, et al., Water chemistry on model ceria and Pt/ceria catalysts, J. Phys. Chem. C 116 (2012) 12103–12113, http://dx.doi.org/10.1021/jp302229x.
[27] S. Benkoula, O. Sublemontier, M. Patanen, C. Nicolas, F. Sirotti, A. Naitabdi, et al., Water adsorption on TiO_2 surfaces probed by soft X-ray spectroscopies: bulk materials vs. isolated nanoparticles, Sci. Rep. 5 (2015) 15088, http://dx.doi.org/10.1038/srep15088.
[28] T. Gouder, R. Eloirdi, R. Caciuffo, Sci. Rep. 8 (2018) 8306, http://dx.doi.org/10.1038/s41598-018-26594-z.
[29] D.A. Shirley, High-resolution X-ray photoemission spectrum of the valence bands of gold, Phys. Rev. B 5 (1972) 4709–4714.
[30] R.J. McEachern, D.C. Doern, D.D. Wood, The effect of rare-earth fission products on the rate of U_3O_8 formation on UO2, J. Nucl. Mater. 252 (1998) 145–149, http://dx.doi.org/10.1016/S0022-3115(97)00286-9.
[31] B. Chen, Y. Ma, L. Ding, L. Xu, Z. Wu, Q. Yuan, Reactivity of hydroxyls and water on a CeO_2 (111) thin film surface: the role of oxygen vacancy, J. Phys. Chem. C 2 (2013) 5800–5810.
[32] A. Seibert, T. Gouder, F. Huber, Interaction of PuO_2 thin films with water, Radiochim. Acta 98 (2010) 647–657.
[33] T. Griffiths, H. Hubbard, M. Davies, Electron transfer reactions in non- stoichiometric ceria and urania, Inorg. Chim. Acta 225 (1994) 305–317.
[34] Y. Hinatsu, T. Fujino, J. Solid State Chem. 73 (1988) 348.
[35] Y. Hinatsu, T. Fujino, J. Less-Common Metals 149 (1989) 197.
[36] M.R. Antonio, U. Staub, J.S. Xue, L. Soderholm, Chem. Mater. 8 (1996) 2673.
[37] K.I. Maslakov, Y.A. Teterin, A.J. Popel, A.Yu. Teterin, K.E. Ivanov, S.N. Kalmykov, V.G. Petrov, P.K. Petrov, I. Farnan, Appl. Surf. Sci. 448 (2018) 154–162.